



# An analytical damage tolerance method accounting for delamination in compression-loaded composites

Raffael Bogenfeld\*, Sebastian Freund, Andreas Schuster

German Aerospace Center, Institute for Composite Materials and Adaptive Systems, Lilienthalplatz 7, 38108 Braunschweig, Germany



## ARTICLE INFO

### Keywords:

Damage tolerance  
Delamination  
Damage growth  
Preliminary aircraft design

### MSC 2019:

00–01  
99–00

## ABSTRACT

An efficient damage tolerance (DT) analysis method is required for application during the preliminary design phase of a composite structure. In the present work, we describe an analytical, energy-based DT analysis method for compression-loaded composite laminates containing a delamination. Based on the sublaminar buckling as the driving phenomenon, the strain energy release rate is calculated through the virtual crack extension method. The consideration of the load transfer within the laminate allows calculating the strain energy release rate in two directions which permits an assessment of the damage propagation direction. Further, the developed method permits taking into account the effects of the laminate width and the damage eccentricity. The obtained results are compared with other analysis approaches and validated through experiments from the literature. This validation approves the method's capability to assess the residual laminate properties, although the method turned out to be less accurate than methods presented in the literature.

## 1. Introduction

Maintaining the structural integrity is a vital need to any transport aircraft. Damage occurring to the aircraft during the service life must not result in catastrophic failure. To comply with this need, particular design philosophies for aircraft structures account for possibly occurring damage. The state of the art philosophy for most aircraft structures is Damage Tolerance (DT) [1,2]. A damage-tolerant design demands the expected damage to be taken into account as early as possible during the design phase. The design has to ensure that the damage cannot infringe the structural integrity for predefined service intervals, which have to be evidenced as DT-safe. When the end of a design interval is reached an inspection has to be scheduled. The discovery of a DT-critical damage has to entail the repair or the replacement corresponding component, to ensure the airworthiness for the further service life.

The DT analysis methods are well-established for designing structures made from metallic materials [3,4]. For structures made from composite laminates, the established, metal-specific DT methods cannot be directly transferred. The damage behavior of composite materials differs significantly from that of metallic materials. While the failure of metals is characterized by through-thickness cracking, composite laminates exhibit a variety of damage modes. The most significant modes are fiber failure, inter-fiber failure, and delamination. Among these damage types, the delamination is particularly critical to a compression-loaded composite structure, as for example Kevin O'Brien describes as early as 1988 [5]. As a delamination is located inside the laminate and hardly visible from the outside, its detectability through a visual inspection cannot be ensured [6].

However, the crucial demand for the reliability of an aircraft structure applies also to composites. According to Newaz and

\* Corresponding author.

E-mail address: [raffael.bogenfeld@dlr.de](mailto:raffael.bogenfeld@dlr.de) (R. Bogenfeld).

<https://doi.org/10.1016/j.engfailanal.2020.104875>

Received 30 March 2020; Received in revised form 7 August 2020; Accepted 21 August 2020

Available online 13 September 2020

1350-6307/ © 2020 Elsevier Ltd. All rights reserved.

Sierakowski, composite structures have to “equal or exceed” [7] the safety standards of a conventional metal structure. Therefore, the public authorities define the possible methods to account for the required DT of composites: the guidelines by the Federal Aviation Administration (FAA) are provided in the Advisory Circular AC 20-107B [8], the guidelines by the European Aviation Safety Agency (EASA) in the Decision No 2010/003/R [9,10]. Briefly summarized, there are three admissible concepts which can be applied to approve the DT. These concepts differ in their permissible damage growth behavior over the service life: *slow growth*: a damage may grow slowly and stably; *arrested growth*: the damage growth has to be self-arresting; *no-growth*: a damage may not grow.

Among these admissible concepts, a strict no-growth approach currently seems to be the only viable method to deal with delamination under compression load. The phase of stable damage growth before the ultimate collapse is too short to permit a slow growth design [11–14]. Only the prohibition of any damage propagation during the entire structural life seems to meet the allowances by the public authorities [15,16]. A special detailed inspection method [17,18] or structural health monitoring [19,20] has to be employed to detect damage as required for a slow growth design. In practical application, the no-growth policy is realized through maximum allowable strain limits, which may never be exceeded [21,22]. The corresponding DT analysis reduces to a residual strength analysis, as stated for example by Sebaey et al. [23] or Dubary et al. [24].

Due to the different behavior of delamination under compression and tension [25,26], the load case determines the driving damage mode for the damage-tolerant design. Delamination is particularly critical to the compression strength as sublaminates are prone to local buckling under compression [5]; so-called sublaminates buckling. The sublaminates buckling crucially influences the global buckling and commonly initiates the structural failure [27–29]. The common determination procedure for the corresponding knock down factors is based on “extensive test campaigns” [30], consisting mainly of compression after impact (CAI) coupon tests [31]. A sufficient residual strength has to be ensured for the service life of a structure. Hence, residual strength testing after cyclic loading is required [32,8].

The elaborate experimental effort to evaluate the DT cannot be managed in the preliminary design phase. Hence, the available test data for specific laminates limits the design space if the conventional procedure is used. A more flexible DT assessment method enhances the design process through the tailored calculation of DT allowables. These tailored allowables are potentially less conservative than a general test-based strain limit. With regard to such a flexible method for the application in the preliminary design phase, a fast DT evaluation is mandatory [33,34]. This requirement leads to the investigation of analytical methods accounting for the DT of delamination under compression load.

1.1. Toward a damage tolerance method for composite laminates

A standard DT analysis of a metallic structure is conducted in a procedure of several steps as depicted in Fig. 1a. Based on a load spectrum, the stress and strain in the structure has to be determined for the unique load states. Usually, a finite element analysis is the method of choice for this determination. In a fracture-mechanical analysis, the strain energy release rate (SERR)  $G$  at the crack tip is determined. The SERR is a fracture-mechanical parameter which is obtainable for each crack tip and load state. The exceeding of the critical SERR  $G_c$  marks the residual strength. For cyclic loading with subcritical values of  $G$ , a crack growth law like the Paris law [35] can be employed which calculates a crack growth rate  $\frac{da}{dN}$  [36,37]. The law’s evaluation for all load amplitudes in the service life enables the calculation of the damage size history over that time. Based on this information, the margin of safety can be calculated either through the residual strength or through the safe damage growth interval.

A DT analysis procedure for compression-loaded composite laminates with delamination can follow the same basic principle as the established DT process for metallic structures (cf. 1) b. When the SERR is determined, the safety margin results from the calculated no-growth interval until the onset of delamination propagation. A crucial difference in the process emerges in the fracture-mechanical analysis step. The determination of the SERR at a through-thickness crack in isotropic material is a single analytical formula based on the state of stress [4]. In contrast to that, the opening of a delamination crack occurs differently. Only for particular delamination

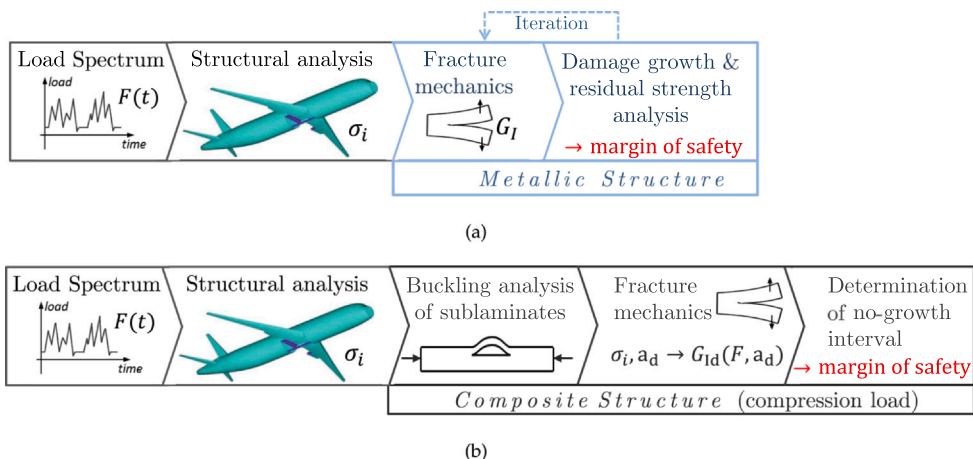


Fig. 1. Steps to be conducted in a DT analysis of a metallic (a) and a composite (b) aircraft structure.

cases, with a clearly defined mode I or mode II crack opening, a direct calculation of the SERR is possible [38–40]. Such a case is the delamination propagation in a double cantilever beam as described in the studies of Krueger [36] and Gbaguidi [37]. However, the determination of the SERR is complex with regard to a compression-loaded laminate with a delamination. The delamination crack front surrounds the delaminated area. The value of the SERR can vary along this crack front. Hence, the DT analysis of a delaminated composite has to be two-dimensional, as proposed by Choudhry et al. [41].

A numerical high-fidelity analysis can be conducted to assess the mechanisms around the delamination under compression load. Examples of such analysis method are shown by Dienel et al. [28,42] or by Riccio et al. [43]. Detailed high-fidelity methods accurately determine the residual strength, however, they are computationally costly and require significant modeling effort. An alternative approach with low computational cost was proposed by Köllner et al. [44]. Their calculation is based on the classical laminate theory (CLT) and analytical plate equations which results in plausible prediction of the delamination growth onset. Nonetheless, the method is limited to circular geometries of the plate and the delamination. A more flexible method has been developed by Rhead, Butler et al. [45–48]. They identified the sublaminates buckling as the driving phenomenon for the compression-driven delamination propagation. Based on the sublaminates buckling, these researchers developed an analysis method for the DT of composite laminates. According to the process in Fig. 1b, their analysis begins with a numerical determination of the sublaminates buckling. Subsequently, the SERR of the buckled delamination is determined analytically. The comparison of the respective results with experimental data affirms the plausibility [45]. As a purely analytical variant, Rhead and Butler propose a one-dimensional beam model for the determination of the sublaminates buckling. However, this beam-based determination provides a rough estimate which is not conservative. In a recent development published in 2019, Choudhry, Rhead et al. present an enhancement of their method which allows a two-dimensional based on plate equations [41]. This enhanced method permits the calculation of the SERRs for elliptical delaminations parallel and perpendicular to the load axis.

The semi-analytical methods proposed by Rhead, Butler, Choudhry et al. fulfill the requirements for a DT assessment of composite structures. The further development to be achieved with this paper shall fit the needs for an application in preliminary aircraft design. To move the DT analysis to a structural level, an efficient analysis should take the load transfer in the structure into account. Also the eccentricity of damage has to be considered to account for an elevation of the damage influence. For that purpose, an analytical two-dimensional analysis to calculate a DT allowable is presented.

## 2. Methods

### 2.1. A fracture-mechanical energy method

The determination of the SERR at the delamination crack tips is key to the DT analysis of composite laminates. According to the findings of Rhead and Butler, we consider the crack opening to be driven by the sublaminates buckling [45]. This crack opening is likely to be a mixed-mode phenomenon [38]. To simplify the analysis, we assume the crack opening as a pure mode I peeling. The critical SERR of mode I is a lower bound for a critical mixed-mode value [49]. With this assumption, an approximation of the mode-mixity can be avoided. The mentioned approaches by Rhead, Butler et al. also employ this practice in order to avoid a mixed-mode criterion [47,41].

To describe the SERR analytically, we need to determine the energy balance of the loaded laminate with the delamination. For each loaded structure, an elastic potential  $\Pi$  can be defined, which is composed of the internal energy  $U$  and the negative external work  $W_e$ . According to Griffith [50], the SERR is the decrease of this elastic potential  $\Pi$  caused by a crack surface increase. This crack

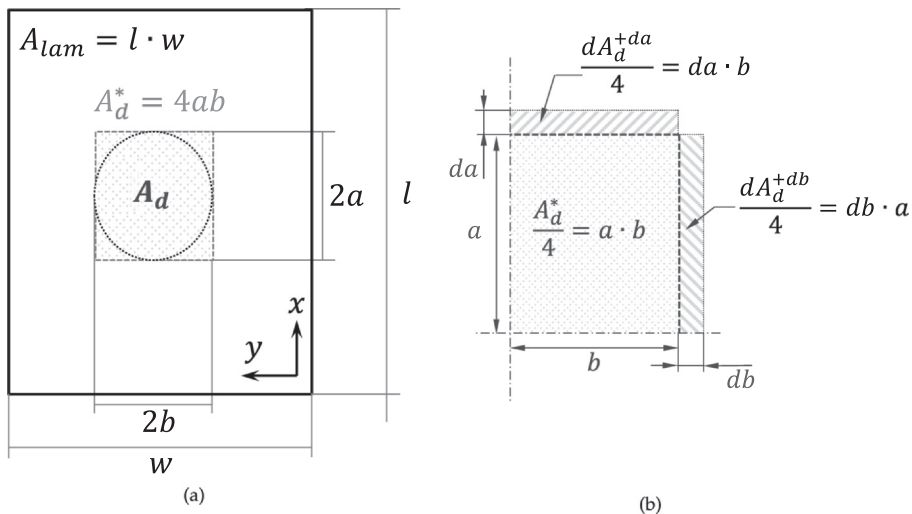


Fig. 2. Geometry of a sample laminate with the area  $A_{lam}$  containing a delamination  $A_d$  with the enveloping area  $A_d^*$  (a) and the virtual extension of the delamination envelope in  $x$ - and  $y$ -direction (b).

surface in Eq. (1) is represented by the delamination area  $A_d$ , in the context of the present analysis (cf. Fig. 2a).

$$G = -\frac{d\Pi}{dA_d} = \frac{dW_e}{dA_d} - \frac{dU}{dA_d} \quad (1)$$

Consequently, the energy values  $W_e$  and  $U$  have to be determined for the loaded laminate. In consideration of the control loop of the load application, the value of  $W_e$  is zero for displacement-control, with constant external displacement  $x_{ext}$ , and the calculation of the SERR simplifies according to Eq. (2). External work is relevant only when the external displacement can change. Hence, for a force-controlled load application, with constant loading  $n$ , Eq. (3) describes the SERR calculation. The respective external work  $W_e$  results from the external load  $n$  and the width of the specimen  $w$  according to Eq. (4).

$$(G)_{x=const.} = \frac{d}{dA_d}(-U) \quad (2)$$

$$(G)_{n=const.} = \frac{d}{dA_d}(W_e - U) \quad (3)$$

$$W_e = \int \mathbf{n} w d\mathbf{x}_{ext} \quad (4)$$

With regard to the crack surface, we introduce a major simplification for the analytical model in this work. Instead of the real delamination area  $A_d$ , the rectangular envelope  $A_d^*$  around the delamination is used for the analysis as shown in Fig. 2a. The length and width of the delamination in x- and y-direction,  $2a$  and  $2b$ , determine the edge lengths of the rectangle, respectively. For circular delamination and elliptical delamination with  $0^\circ$  or  $90^\circ$  orientation the relation of the surfaces is  $A_d^* = \frac{4}{\pi}A_d$  which is an increase of 27%. Nonetheless, there are reasons to question this rectangular approximation. First, an inclined ellipse, results in a surface increase which depends on the aspect ratio of the ellipse. The increase can be much larger than the above calculated 27%. Second, the qualitatively different shape of the damage could possibly affect the mixed-mode ratio at the crack tips. Hence, a plausible prediction of the mixed-mode behavior could not be ensured if it was considered.

The authors intend the rectangular envelope to exhibit a conservative damage growth threshold in comparison to the real elliptical damage. The arguments in favor of the conservatism are the area enlargement and the fact that the growth of a rectangular delamination results in a nearly elliptical delamination shape with two tips perpendicular to the load direction [51]. Hence, according to the thermodynamic principle of minimum energy, the elliptical shape is considered to be preferential to the rectangular shape. Nonetheless, an argument against the conservatism is a possible load peak concentration at the lateral delamination tips, which is not existent for the rectangular shape. Eventually, the conservatism is neither analytically nor empirically proven in this work.

On the basis of  $A_d^*$ , the virtual crack extension method enables the calculation of the SERR according to Eq. (3). The virtual crack extension can be conducted separately in the x- and the y-direction, which permits to distinguish the SERR in parallel and perpendicular direction to the load axis. The virtual enlargement of the delamination is assumed by increasing the delamination area  $A_d^*$  through the parameters  $a$  and  $b$ . This virtual extension by a small increment  $da$  or  $db$  extends the delamination area to the values  $dA_d^{+da} = 4(a + da)b$  or  $dA_d^{+db} = 4a(b + db)$ , as depicted in Fig. 2b. The energy quantities  $W_e$  and  $U$  are functions of the delamination area and calculated accordingly. Instead of the differential derivative in Eq. (1), the difference quotient shown in Eq. (5) is evaluated. The calculation of the laminate's energy quantities is, thus, conducted twice: first, for the current delamination size  $A_d^*$ , second, for a virtually enlarged size  $A_d^{+dA}$ . The virtual extension by  $da$  and  $db$  has to be conducted separately. Accordingly, two SERRs in perpendicular directions can be calculated,  $G_x = -\frac{d\Pi}{dA_d^{+da}}$  and  $G_y = -\frac{d\Pi}{dA_d^{+db}}$ .

$$(G)_{n=const.} = \frac{(W_e^+ - U^+) - (W_e - U)}{\Delta A_d^*} = \frac{(W_e^+ - W_e) + (U - U^+)}{\Delta A_d^*} \quad (5)$$

## 2.2. Energy in the pristine laminate sections

The virtual crack extension requires a calculation procedure for the internal energy in the delaminated laminate. The internal energy of the laminate is calculated through the stress-strain integral of the laminate with the area  $A_{lam}$  (cf. Eq. (6)). According to the CLT, the laminate deformation state is described through the membrane and plate effects. These lead to a replacement of  $\sigma$  and  $\epsilon$ . The load vector  $\mathbf{n} = \begin{pmatrix} \mathbf{N} \\ \mathbf{M} \end{pmatrix}$  describes the membrane end bending forces, the respective degrees of freedom are included in  $\mathbf{x} = \begin{pmatrix} \epsilon \\ \kappa \end{pmatrix}$ . These vectors are related according to the basic equation of the CLT in Eq. (7) and Eq. (6) can be rearranged to Eq. (8), where  $\begin{pmatrix} \mathbf{N} \\ \mathbf{M} \end{pmatrix}$  is the integrand. For a homogeneously deformed laminate with linear elasticity, the energy integral simplifies to an elementary matrix multiplication in Eq. (8).

$$U = A_{lam} \int_0^{t_{lam}} \int_0^e \sigma d \epsilon dz = A_{lam} \left[ \int_0^e \mathbf{N} d\hat{\epsilon} + \int_0^k \mathbf{M} d\hat{\kappa} \right] \quad (6)$$

$$\begin{pmatrix} \mathbf{N} \\ \mathbf{M} \end{pmatrix} = \begin{pmatrix} \mathbf{A} & \mathbf{B} \\ \mathbf{B} & \mathbf{D} \end{pmatrix} \begin{pmatrix} \epsilon \\ \kappa \end{pmatrix} \quad (7)$$

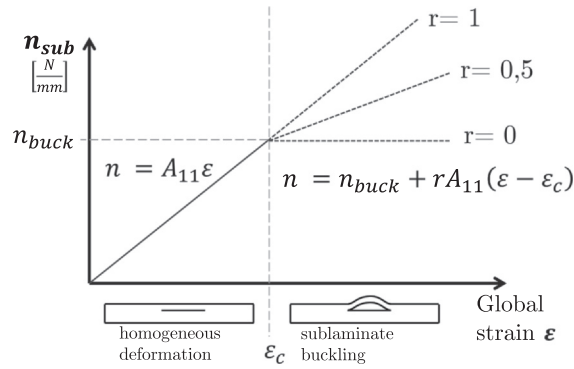


Fig. 3. Load-deformation curve of a sublaminates before and after delamination buckling.

$$U = A_{lam} \int_0^{\begin{pmatrix} \varepsilon \\ \kappa \end{pmatrix}} \begin{pmatrix} \mathbf{N} \\ \mathbf{M} \end{pmatrix} d \begin{pmatrix} \hat{\varepsilon} \\ \hat{\kappa} \end{pmatrix} = \frac{1}{2} \begin{pmatrix} \varepsilon \\ \kappa \end{pmatrix}^T \begin{pmatrix} \mathbf{A} & \mathbf{B} \\ \mathbf{B} & \mathbf{D} \end{pmatrix} \begin{pmatrix} \varepsilon \\ \kappa \end{pmatrix} A_{lam} \quad (8)$$

### 2.3. Internal energy of delaminated laminates

The energy calculation according to Eq. (8) is valid only for homogeneously deformed laminates. However, a laminate containing a delamination cannot be considered as entirely homogeneous. Hence, several distinctions are necessary: a sequential distinction of load sections and a spatial distinction of differently loaded specimen areas.

#### 2.3.1. The laminate response before and after sublaminates buckling

A sequential distinction of the load sections has to be conducted as the occurrence of buckling significantly affects the energy distribution. First, the damaged and the undamaged area deform homogeneously. Up to the sublaminates buckling load  $n_{buck}$  and the respective critical strain  $\varepsilon_c$ , the deformation is linear elastic (cf. Eq. (9)). This homogeneity disappears as soon as one sublaminates buckles.

The energy stored in a buckling sublaminates has to be calculated. This calculation requires an assumption about the post-buckling stiffness of a sublaminates. The work of Diaconu and Weaver [52] suggests a linear decrease of the stiffness in load direction according to Eq. (10) as the diagram in Fig. 3 shows. Considering these published experiments, Rhead et al. suggest the range  $0.35 < r < 0.65$  for orthotropic laminates. However, their study is conducted using two values;  $r = 0.5$  for approximating the real behavior, and  $r = 0$  representing a lower bound which results in the largest SERR. For the analyses presented in the current article the value is set to zero,  $r = 0$ .

The sequential distinction requires determining the buckling strain  $\varepsilon_c$  of each sublaminates. In this regards, the existing method by Rhead and Butler [45,47,22] uses a numerical buckling analysis or a simplified one-dimensional beam model. To match the needs of the preliminary-design phase, the model presented in this work requires an efficient buckling determination. This requires either to substitute a numerical model with a predetermined response surface or to employ an analytical method. As the a priori determination and the interpolation in the discrete design space of stacking sequences is complex [53], the direct calculation through analytical equations was preferred. An analytical plate buckling correlation for rectangular, orthotropic plates with different boundary conditions suits the calculation of the sublaminates buckling. Such equations are, for example, provided in the publication by Tarjan and Kollar [54] or in the structural analysis manual HSB Section 45000 [4]. Both approaches are outlined in the Appendix A.

$$n_{buck} = A_{11sub} \varepsilon_c \quad (9)$$

$$\Delta n_{11sub} = r A_{11sub} \Delta \varepsilon_{11} \quad (10)$$

#### 2.3.2. Spatial distinction of the energy calculation

A spatial distinction of the sublaminates and the pristine laminate is necessary. First, the energies of the pristine laminate and both sublaminates in the delaminated area  $A_d^*$  have to be calculated separately. The pristine laminate's elastic energy can still be calculated according to Eq. (8). The same also applies to the energy calculation of the non-buckling sublaminates. The corresponding segmentation of the specimen in separate regions is depicted in the Fig. 4. This segmentation is chosen to account for the load transfer caused by the sublaminates buckling. The load decrease in the buckling sublaminates causes a load increase in the base laminate under the delamination (second sublaminates) and in the left and right sections. Eventually, we differentiate six regions of the specimen as the Fig. 4 shows. In each region, the internal energy has to be calculated. In Eq. (11), the sum of all six internal energy values results in the quantity  $U$ .

$$U = U_{up} + U_{down} + U_l + U_r + U_{sub1} + U_{sub2} \quad (11)$$

The values in the upper and the lower section of the specimen,  $U_{up}$  and  $U_{down}$ , can directly be obtained through Eq. (8). The respective

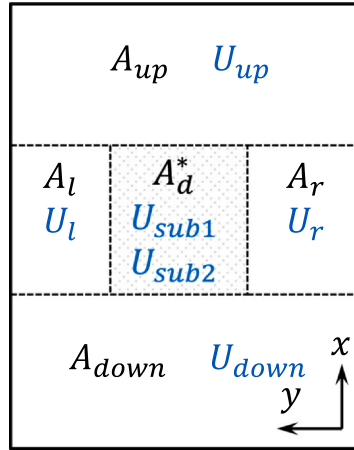


Fig. 4. The segmentation of the specimen into regions for the energy calculation including the respective energy quantities (blue).

areas are defined through the specimen geometry and sustain the applied line load  $n_{11}$ . Using the same principle, we can calculate interim values  $\tilde{U}_l$  and  $\tilde{U}_r$  for the side sections to the left and to the right of the delamination. For this case, the values  $\tilde{n}_l$  and  $\tilde{n}_r$  are equal to  $n_{11}$ . These interim values are only valid for plates of infinite width  $w \rightarrow \infty$ . In a real plate, the load in the side sections increases through the load transfer from the delaminated section. Due to their dependence on the load in the buckling sublaminde, the real energy values  $U_l$  and  $U_r$  can only be calculated after the determination of the sublaminde buckling. Trivially, the same applies to the sublaminde energies.

2.3.3. Energy in a buckled sublaminde

The occurrence of buckling substantially changes the deformation of the respective sublaminde. Accordingly, the calculation procedure of  $\tilde{U}_{sub1/2}$  has to be adapted as the CLT does not suit to describe the deformation. As Rhead stated [45], the sublaminde buckling is dominated by nonuniform bending instead of uniform membrane deformation. This deformation results in an energy density which is not constant. Hence, an integral approach needs to account for these effects. Instead of an energy integral over the delaminated area, the external work by the section force  $\tilde{n}_{sub1/2}$  on the delamination boundary provides the basis for the energy calculation. This force-based approach is one-dimensional, hence it is not applicable for multidirectional loading. Nonetheless, its advantage is that it only requires the description of the sublaminde’s post-buckling behavior to calculate the energy in the respective region. The respective post-buckling behavior is shown in the diagram in Fig. 3. Accordingly, the energy  $\tilde{U}_{sub1/2}$  can be described by the Eqs. (12) and (13).

$$\Delta \tilde{U}_{sub1/2} = 2a \cdot \Delta \varepsilon_{11} \cdot \frac{\tilde{n}_{sub1/2} + n_{buck1/2}}{2} \cdot 2b \tag{12}$$

$$\tilde{U}_{sub1/2} = \frac{2a \cdot 2b \cdot \varepsilon_c \cdot n_{buck1/2}}{2} + 2a \cdot \underbrace{(\varepsilon_{11} - \varepsilon_c)}_{\Delta \varepsilon_{11}} \left( n_{buck1/2} + \frac{rA_{11sub1/2} (\varepsilon_{11} - \varepsilon_c)}{2} \right) \cdot 2b \cdot \underbrace{\left( \frac{\tilde{n}_{sub1/2} + n_{buck1/2}}{2} \right)}_2 \tag{13}$$

2.4. Load redistribution

The free cut through the specimen in Fig. 5b shows the acting forces in the pristine and the delaminated regions. From this free cut, the equilibrium of forces in the loading direction reveals an inconsistency of an energy balance with the values  $\tilde{U}_i$ . A pure reduction of the sublaminde section forces  $\sum \tilde{n}_{subi}$  violates the equilibrium of forces in the x-direction (Eq. (14)). The free cut illustrates that the real values  $n_l$  and  $n_r$  cannot be equal to  $n_{11}$ .

$$\sum_i \tilde{n}_{subi} 2b + n_l w_l + n_r w_r = n_{11} w \tag{14}$$

To describe physically consistent load state, one has to account for the load transfer from the buckling sublaminde to the pristine side sections and to the remaining base laminate (second sublaminde). The actual section forces  $n_i$  have to be calculated considering this load redistribution. For that purpose, the equilibrium of the forces in x-direction and the equilibrium of moments are employed.

The calculation is conducted under the assumption that the specimen remains flat after the asymmetric stiffness loss in one sublaminde. Hence, the global bending effect as shown by Rhead et al. in 2017 [22] is not included in the present model, which limits the applicability to cases with restrained edges. Further, the model is based on a uniform load distribution in each specimen

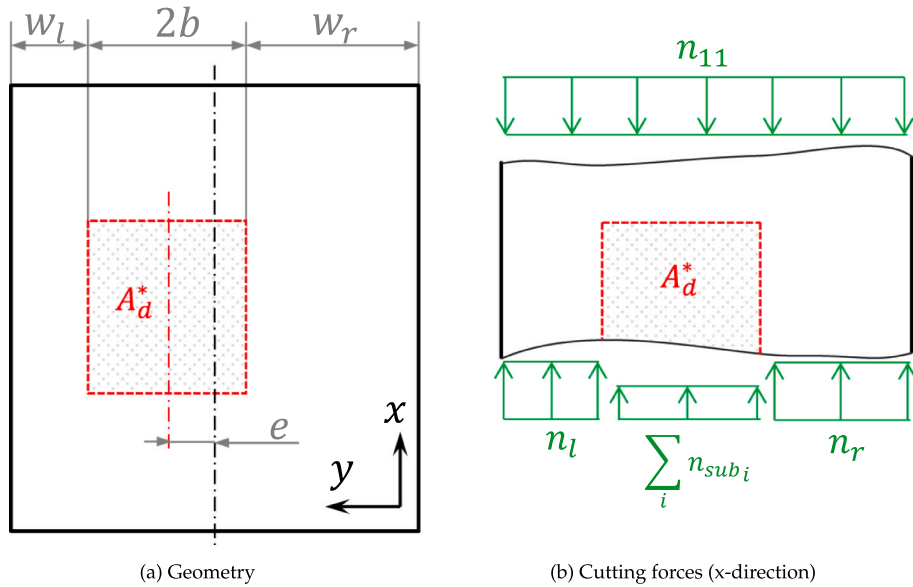


Fig. 5. Sketch of the off-centered delamination geometry and the cutting forces in the pristine and the delaminated cross sections.

section. Through this assumption, the line loads can be replaced by their effective forces attacking at the center of the respective line. The corresponding lever arms of the forces derive directly from the specimen geometry. However, this assumption limits the validity of the analysis approach to a uniform load  $n_{11}$ , as a non-uniform external load would require to consider non-uniform load in the individual cross sections. Notably, further damage-driven stress concentration close to the delamination edge is not included in the presented approach.

The load transfer results from the difference of the sum of the preliminary sublaminate section forces  $\tilde{n}_{sub_i}$  and the applied external load to that section  $2bn_{11}$ . Hence, the load to be redistributed  $\Delta F$  is calculated through (15).

Two steps are conducted to calculate the redistribution. In the first step,  $\Delta\varepsilon_{11}$  the mean strain increase in the damaged cross section is calculated through Eq. (16).

$$\left( \sum_i \tilde{n}_{sub_i} - n_{11} \right) 2b = \Delta F \tag{15}$$

$$\Delta\varepsilon_{11} = \frac{\Delta F}{(w_r + w_l)A_{11lam} + 2b(A_{11sub-non-buckling} + rA_{11for-sub-buckling})} \tag{16}$$

The additional strain  $\Delta\varepsilon_{11}$  increases the sublaminate forces  $n_{sub_{1/2}}$  and the sublaminate energy  $U_{sub_{1/2}}$  according to the Eqs. (17) and (18), respectively. Also the load increase in the side sections can be calculated in similar manner (Eq. (19)). The corrected forces  $n_{sub_{1/2}}$  and  $\tilde{n}_{l/r}$  fulfill the equilibrium of forces, as they contain the redistribution of the load  $\Delta F$ .

$$n_{sub_{1/2}} = \tilde{n}_{sub_{1/2}} + \Delta\varepsilon_{11}A_{11sub_{1/2}} \tilde{r} \begin{cases} \tilde{r} = 1, \text{ for nonbuckling sublaminate} \\ \tilde{r} = r, \text{ for buckling sublaminate} \end{cases} \tag{17}$$

$$U_{sub_{1/2}} = \tilde{U}_{sub_{1/2}} + \frac{n_{sub_{1/2}} + \tilde{n}_{sub_{1/2}}}{2} \Delta\varepsilon_{11} \cdot 4ab \tag{18}$$

$$\tilde{n}_{l/r} = \tilde{n}_{l/r} + \Delta\varepsilon_{11}A_{11} \tag{19}$$

Notably, the approach presented here does not consider any further stress concentration close to the delamination edge. Instead, each line load  $n$  is assumed to be constantly distributed over the respective width. Further, the force  $\Delta F$  is transferred according to  $\Delta\varepsilon_{11}$  to the laminate base and both cross sections to the left and right of the delamination. In case of a centric delamination with  $w_l = w_r$ , the symmetry condition  $n_l = n_r$  suffices as a second equation. Trivially, the respective portions of  $\Delta F$  get transferred equally to both sides and Eq. (19) is correct.

However, in case of an off-centered delamination which is horizontally removed from the middle axis as in Fig. 5, this transfer is not trivial anymore. The eccentricity  $e$  according to the Eq. (20) describes the difference of the vertical center lines of the specimen and the delamination as Fig. 5a shows.

$$e = \frac{w_r - w_l}{2} \tag{20}$$

The equilibrium of moments in Eq. (21) provides the missing second equation in addition to the force equilibrium. To set up this equilibrium condition, we assume uniform line loads in each section. These can be replaced by their resulting forces (cf. Eq. (22)) attacking at the midpoint of the respective lines. Thus, the two equilibrium equations, Eq. (15) and Eq. (21), have to be solved for the two unknowns  $n_l$  and  $n_r$ .

$$0 = \left(\frac{b+e}{2} + \frac{w}{4}\right) \cdot F_l + e \cdot F_{sub} - \left(\frac{b-e}{2} + \frac{w}{4}\right) \cdot F_r \tag{21}$$

$$\begin{aligned} F_l &= \left(\frac{w}{2} - b - e\right) n_l \\ F_r &= \left(\frac{w}{2} - b + e\right) n_r \\ F_{sub} &= 2b \sum_i n_{subi} \\ F_{11} &= w n_{11} \end{aligned} \tag{22}$$

Eventually, the Eqs. (23) show the loads in the side sections, resulting from the system of Eqs. (22). These loads have to be employed to calculate of the SERR. According to the Eqs. (7) and (8), the internal energy correlates quadratically with the load. Thus, the calculation of the respective values for  $U$  in Eq. (24) can be accomplished through a correction factor  $\left(\frac{n_r}{n_{11}}\right)^2$  multiplied with the energy without load redistribution  $\tilde{U}$ .

$$\begin{aligned} n_l &= \frac{F_{11} - \frac{eF_{sub}}{\left(\frac{b-e}{2} + \frac{w}{4}\right)} - F_{sub}}{1 + \frac{\left(\frac{b+e}{2} + \frac{w}{4}\right)}{\left(\frac{b-e}{2} + \frac{w}{4}\right)}} \cdot \frac{1}{w_l} \\ n_r &= \frac{F_{11} + \frac{eF_{sub}}{\left(\frac{b+e}{2} + \frac{w}{4}\right)} - F_{sub}}{1 + \frac{\left(\frac{b-e}{2} + \frac{w}{4}\right)}{\left(\frac{b+e}{2} + \frac{w}{4}\right)}} \cdot \frac{1}{w_r} \end{aligned} \tag{23}$$

$$\begin{aligned} U_l &= \tilde{U}_l \left(\frac{n_l}{n_{11}}\right)^2 \\ U_r &= \tilde{U}_r \left(\frac{n_r}{n_{11}}\right)^2 \end{aligned} \tag{24}$$

### 2.5. External work due to stiffness decrease

The propagation of the delamination decreases the specimen stiffness. Within the damaged specimen cross section, the additional strain component  $\Delta\varepsilon_{11}$  results from this stiffness decrease. The consequence for a constant force loading is a displacement increase at the loading edge which can be calculated through the strain delta multiplied with the damage length,  $x_{ext} = \Delta\varepsilon_{11} 2a$ . In case of an eccentricity  $e \neq 0$ , the average strain increase has to be recalculated through Eq. (25). Due to the quadratic correlation of the strain and the energy, this equation uses a weighted quadratic mean of the load increase in the side sections. For the symmetrical case of  $e = 0$ , the average external strain increase  $\Delta\varepsilon_{11}^*$  is equal to  $\Delta\varepsilon_{11}$ , the strain increase in the damaged cross section.

$$\Delta\varepsilon_{11}^* = \Delta\varepsilon_{11} \sqrt{\frac{w_l \left(\frac{n_l}{n_{11}}\right)^2 + w_r \left(\frac{n_r}{n_{11}}\right)^2}{w_r + w_l}} \tag{25}$$

According to Eq. (4), the external work is the integral of the load and the displacement at the loading edge. For damage propagation under force controlled loading, the differences in the external energy  $W_e$  emerges through the difference of the external displacement  $dx_{ext} = x_{ext}^+ - x_{ext}$ . The respective displacement differences  $dx^{+db}$  and  $dx^{+db}$  can be calculated from the differences of the external displacement  $x_{ext}$  at the loading edge (cf. Eq. (26)). The resulting displacement increase  $dx_{ext}$  permits calculating the respective values for the external energy difference  $dW_e$ , as given in Eq. (27).

$$x_{ext} = l\varepsilon_{11} + 2a\Delta\varepsilon_{11}^* \tag{26}$$

$$\begin{aligned} dW_e^{+da} &= n_{11} \cdot w \cdot dx_{ext}^{+da} \\ dW_e^{+db} &= n_{11} \cdot w \cdot dx_{ext}^{+db} \end{aligned} \tag{27}$$

In case of a displacement controlled loading, by definition, the decrease of the specimen stiffness does not cause any displacement increase. Instead, the load decreases, according to Hooke's law. This effect is neutral to the external energy balance, resulting in an external work difference of zero for displacement control.

**Table 1**

Overview of the experimental test cases from the literature.

Label	Layup incl. delamination <sup>a</sup>	Specimen $l \times w$ [mm <sup>2</sup> ]	Damage diameter [mm]	Material	Source
R1	[45, 0]   - 45, 90, 45, 0, -45, 90]S	205 × 100	27	AS4/8552	[56,45]
R2	[45, -45, 0]   90, 45, -45, 0, 90]S	250 × 50	15	XAS/914	[45]
R3	[90, -45, 45, 0, 90]   - 45, 45, 0, (0, 45, -45, 90)S]3	250 × 156	50	HTA/6376	[57,45]
R4	[±45, 0, 90, 45]   - 45, 0 <sub>2</sub> , ±45, 0, 90, ±45, 0, 90, ±45, 0 <sub>2</sub> , ±45, 0, 90]S	250 × 156	50	HTA/6376	[57,45]
C1	[0, 0, 90]   45, -45, 45, -45, 90]S	210 × 100	39	T700/M21	[48,41]
C2	[0, 0]   45, -45, 90, 45, -45, 90]S	210 × 100	39	T700/M21	[48,41]
C3	[15, 30]   - 30, -15, 0, 90, 90, 0]S	210 × 100	39	T700/M21	[41]
C4	[0, 90, 90]   45, -45, 45, -45, 0]S	210 × 100	39	T700/M21	[48,41]
C5	[90, 0, 90]   45, -45, 45, -45, 0]S	210 × 100	39	T700/M21	[48,41]
C6	[90, 90, 0]   45, -45, 45, -45, 0]S	210 × 100	39	T700/M21	[48,41]
C7	[0, 45]   0, -45, 90, 45, -45, 90]S	210 × 100	39	T700/M21	[48,41]
C8	[15, 60]   - 60, -15, 0, 90, 90, 0]S	210 × 100	39	T700/M21	[41]
C9	[30, -30]   0, 90, 90, 0, 90, 0]S	210 × 100	39	T700/M21	[55,41]
C10	[30, -30]   0, 0, 30, -30, 30, 60, -60, 30, -30, 30, 0, 0, -30, 30]S	210 × 100	39	T700/M21	[55,41]
C11	[45, 45]   - 45, -45, 90, 0, 90, 0]S	210 × 100	39	T700/M21	[48,41]
C12	[45, -45]   0, 0, -45, 90, 45, 90]S	210 × 100	39	T700/M21	[48,41]

<sup>a</sup> Two vertical lines || indicate the separation of the sublaminates in the damaged region. Each layup contains exactly one delamination, hence, the indicated layup symmetry/ multiplication does not apply to this damage indicator.

### 2.6. Strain energy release rates at the delamination front

Using the derived equations for the internal energy and the external work, we obtain the SERRs through Eq. (5). Therefore, the energy quantities have to be calculated for the current damage state  $[a, b]$  and for the virtually extended damages  $[a + da, b]$  and  $[a, b + db]$ . The values  $G_x$  and  $G_y$  are given in the Eqs. (28) and (29).

$$G_x = \frac{n_{11}W(x^{+da} - x) + (U - U^{+da})}{2(2 \cdot b \cdot da)} \quad (28)$$

$$G_y = \frac{n_{11}W(x^{+db} - x) + (U - U^{+db})}{2(2 \cdot a \cdot db)} \quad (29)$$

These SERRs can be used for a damage propagation analysis, for example through a Paris law [36,37]. Nonetheless, a stable crack growth is unlikely for this load case. In accordance with the no-growth approach, a fatigue law for the determination of the crack growth onset can be employed. Such a modification even simplifies the analysis procedure as an update of the delamination geometry during the analysis is not necessary.

## 3. Results and discussion

For the application of the developed model, several test cases with experimental reference data are taken from different literature sources. In total, a set of 16 configurations (R1 – R4 and C1 – C12) as shown in the Table 1 forms the basis of reference cases to be analyzed through the current model. The list of test cases includes laminates manufactured from four different CFRP prepreg materials: *Hexcel T700/M21*, *HTA/6376*, *AS4/8552*, and *XAS/914*. The Table 2 provides the relevant material parameters including their sources for all four materials. The referenced test cases were already applied to validate the damage growth models by Rhead, Butler, Choudhry et al. [45,48,55,41]. Therefore, the specimens were manufactured with included artificial delaminations of a specified size. These specimens were subjected to compression tests, where the buckling strain of the sublaminates  $\epsilon_c$  and the threshold strain for damage propagation  $\epsilon_{th}$  were recorded.

**Table 2**

Material parameters for the presented test cases from the literature.

Parameter	T700/M21	HTA/6376	AS4/8552	XAS/914
Source	Butler et al. [48]		Rhead et al. [45]	
$t_{ply}$	0.25 mm	0.13 mm	0.25 mm	0.125 mm
$E_{11}$	136 GPa	133 GPa	128 GPa	135 GPa
$E_{22}$	8.9 GPa	10.8 GPa	10.3 GPa	8.5 GPa
$G_{12}$	4.5 GPa	3.6 GPa	6.0 GPa	6.0 GPa
$\nu_{12}$	0.35	0.3	0.3	0.3
$G_{Ic}$	0.55 MJ/mm <sup>2</sup>	0.24 MJ/mm <sup>2</sup>	0.26 MJ/mm <sup>2</sup>	0.1 MJ/mm <sup>2</sup>

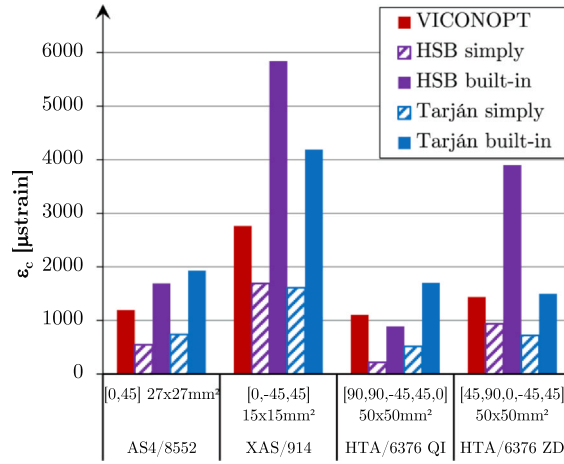


Fig. 6. The sublaminate buckling strain  $\epsilon_c$  calculated through the HSB method [4] and the formula by Tarján et al. [54] in comparison with the VICONOPT results by Rhead et al. [45].

3.1. Calculation of the critical strain for sublaminate buckling

The analysis begins with the determination of the sublaminate buckling strain  $\epsilon_c$ . This strain can be calculated analytically for clamped or simply-supported boundary conditions, either through the approaches from the structural analysis manual HSB or the formulas of Tarján et al., (cf. A). To evaluate the suitability of the approaches, all four variants are employed to calculate the buckling strain  $\epsilon_c$  of four test cases R1 – R4. The respective analysis results for  $\epsilon_c$  are depicted in the diagram in Fig. 6 where they are compared with the results obtained through the numerical tool VICONOPT [58]. This comparison shows, that the boundary conditions assumed at the delamination edges severely influence the critical buckling strain. The assumption of built-in edges leads to an overestimation of  $\epsilon_c$ . In contrast to that, the simply supported plates exhibit a much lower critical strain value than the reference calculation through VICONOPT. In case of a real delamination, the embedding of the sublaminate corresponds to a continuous elastic support. Hence, a built-in boundary condition is stiffer than the real embedding and the prediction of the critical buckling strain is not conservative. In contrast, the simply supported boundary conditions are more compliant than the real embedding and lead to a significant underestimation of  $\epsilon_c$ .

To choose a formula for the buckling strain determination, the influence of the buckling strain on the SERR result of the analysis is studied through the calculation of  $G_x(\epsilon_c)$  and  $G_y(\epsilon_c)$ . For that purpose, the test case C2 is exemplified and analyzed for a strain level of  $\epsilon_{11} = 5000 \mu\text{strain}$  and for three different damage sizes. The diagrams in Fig. 7 depict the result curves. Trivially, the SERR decreases to zero when the buckling strain is equal to  $\epsilon_{11}$ . The maximum SERR values do not necessarily occur for the minimal buckling strain ( $\epsilon_c = 0$ ). Hence, a lower bound buckling strain does not ensure a conservative result for the SERR result. Instead, an accurate determination of  $\epsilon_c$  is key for a plausible estimate in the DT analysis. For that reason, the analytical calculation in the present work is supplied with the average value of the buckling strains for simply supported and built-in edges. The formulas of Tarján et al. are preferred over the variants from the structural analysis manual.

3.2. Threshold strain for delamination propagation

After the initiation of sublaminate buckling, the crack tips begin to open and the SERRs become non-zero. This calculation

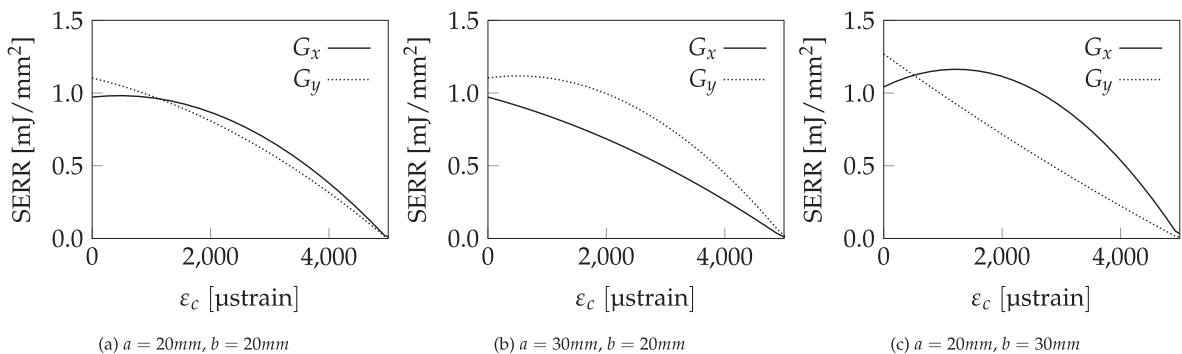
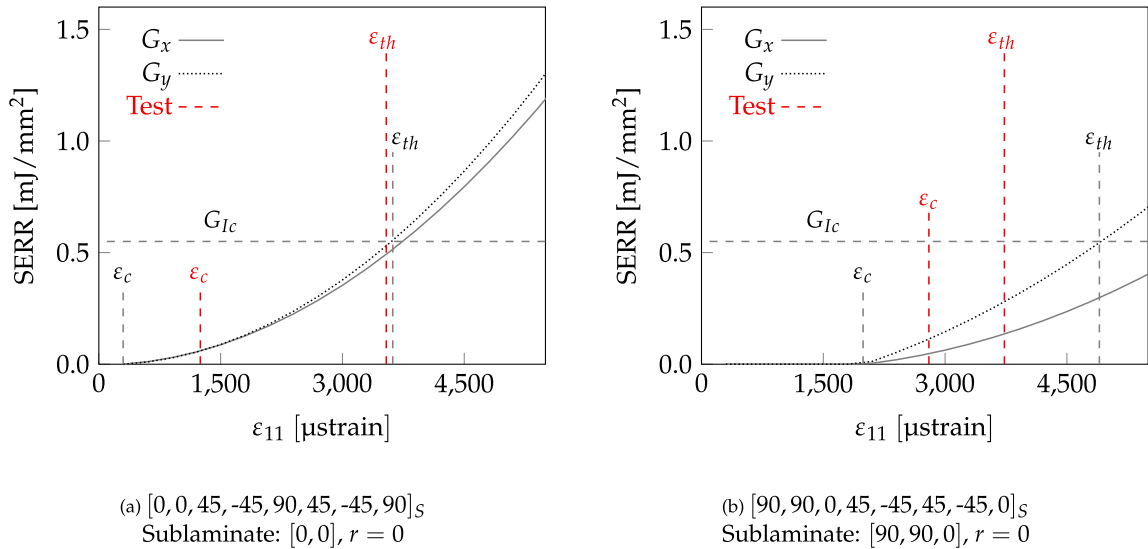


Fig. 7. Energy release rates in x- and y-direction depending on the buckling strain  $\epsilon_c$  for a similar strain level of  $\epsilon_{11} = 5000 \mu\text{strain}$ .



**Fig. 8.** SERR depending on the strain level for two test cases from Butler et al. [48].  $\epsilon_{th}$  represents a conservative estimate of the laminate's residual capacity.

requires a value for  $r$ , to determine the post-buckling stiffness of the sublaminate. In order to reach a conservative estimate,  $r = 0$  is used for all calculations in this section. The Eqs. (28) and (29) from the Section 2.6 are evaluated continuously depending on the strain level  $\epsilon_{11}$ .

The diagram in Fig. 8 depicts the development of the SERR depending on the strain for two sample laminates of the test cases C2 and C6. The SERR values begin to increase after sublaminate buckling initiates. The increase is nonlinear and differs between  $G_x$  and  $G_y$ . The propagation threshold strain  $\epsilon_{th}$  derives from the exceedance of the critical SERR  $G_{Ic}$  by the SERR at any delamination crack tip.

The resulting delamination propagation can possibly be unstable, even though the instability does not directly deduce from this exceedance. The gradient of the SERR has to be checked to assess the stability. Nonetheless,  $\epsilon_{th}$  marks a conservative estimate for the initiation of the damage propagation.

The threshold strain  $\epsilon_{th}$  and the buckling strain  $\epsilon_c$  are calculated for entire set of test cases. The diagram in Fig. 9 depicts these calculation results and the available experimental reference values from the literature sources (cf. Table 1). Further, the analysis results obtained by Rhead et al. [45] and Choudhry et al. [41] are included. With few exceptions, the analytical calculation of the buckling strain reasonably approximates the experimental reference (or the numerical result obtained through VICONOPT). However, several significant underestimations exist.

The results of the damage propagation threshold calculated through the current method reasonably predict the experimental reference. However, the threshold is overestimated for the most cases. Therefore, conservatism cannot be ensured even for  $r = 0$ . Remarkably, the agreement is better for the four test cases R1 – R4. Nonetheless, Rhead et al. reported a better accuracy for these cases. For the further cases C1 – C12 the accuracy of the current method is worse, as most results are clearly above both the experimental reference and the result by Choudhry et al. A possible explanation could be the applied value of  $G_{Ic} = 0.55 \text{ mJ/mm}^2$ , which originates from the experiments of Ilyas et al. [59]. However, Choudhry et al. mention a second  $G_{Ic} = 0.33 \text{ mJ/mm}^2$  as reported in [60]. Hence a systematic deviation due to the critical SERR value could be a possible explanation of the overestimation seen for the cases C1 – C12.

### 3.3. Dependency on the specimen width and the damage eccentricity

The behavior of  $G_y^l$  and  $G_y^r$  and  $G_x$  depends on the specimen width  $w$  and the eccentricity  $e$  of the delamination. To study these dependencies, the test case C2 is subjected to a strain level of  $\epsilon_{11} = 2500 \mu\text{strain}$ . The specimen width and the damage eccentricity, as the parameters of interest, are accordingly modified. For a qualitative investigation, dimensionless parameters are derived for the relative specimen width and the relative eccentricity.

The specimen width is normalized through the damage width,  $\frac{w}{2b}$ . This dimensionless variable approaches 1 when the damage comprises the entire specimen width. The diagram in Fig. 10a shows an increase of both  $G_x$  and  $G_y$  for a small width to damage ratio. The load transfer from the damaged cross section to the pristine side sections explains this observed behavior. Remarkably, the SERR in load direction,  $G_x$  becomes larger than the lateral value  $G_y$  for a large width to damage ratio. The reason for this behavior can be found in the energy calculation in the side sections of the plate. The corresponding correction factors are calculated based on a homogeneous distribution of the load in the side sections. While this leads to a significant increase of the energy density for small ratios  $\frac{w}{2b}$ , a large ratio corresponds to hardly any load increase in the side sections. Hence, the correction factors in Eq. (24) are close

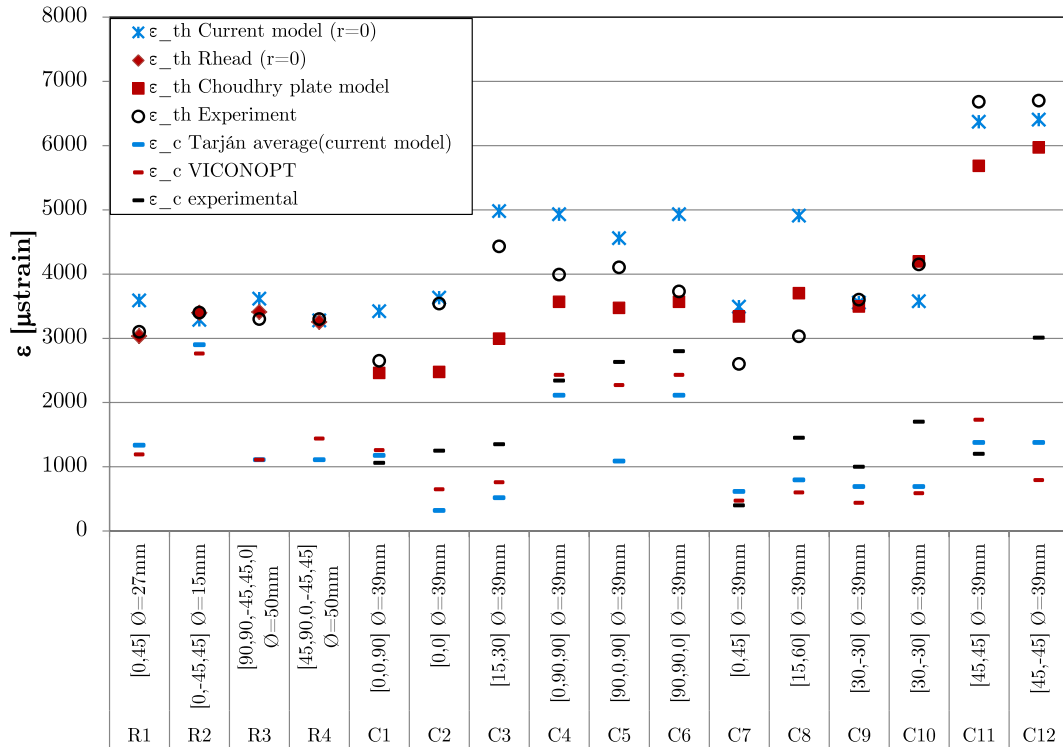
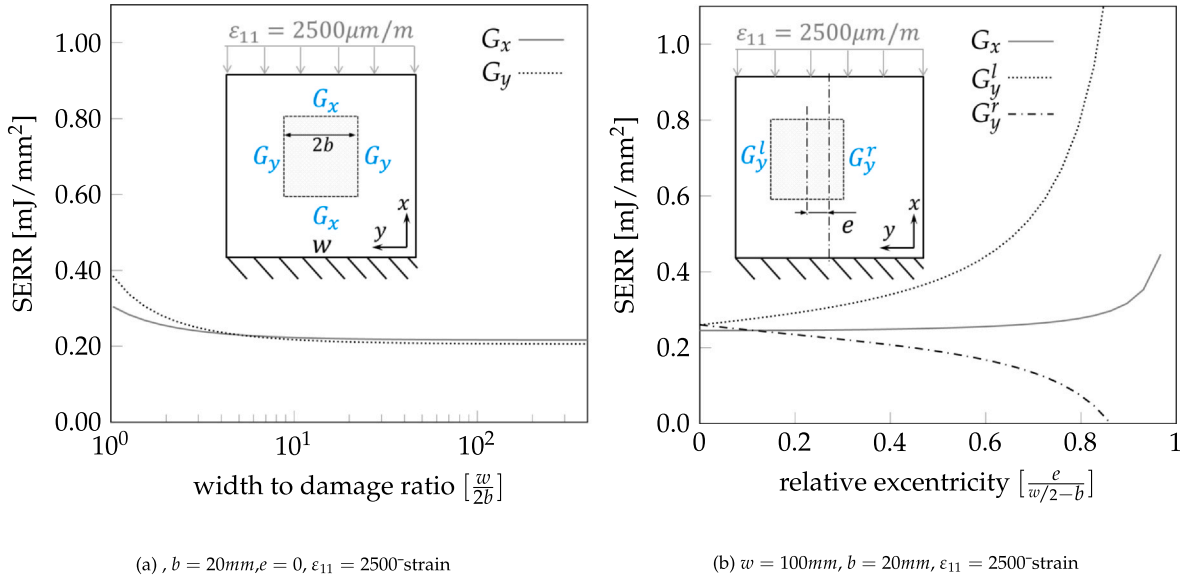


Fig. 9. Results for the threshold strain for damage growth  $\epsilon_{th}$  in comparison of the present model (blue) and the results reported by Rhead et al. [45] and Choudhry et al. [41]. (For interpretation of the references to colour in this figure legend, the reader is referred to the web version of this article.)



(a) ,  $b = 20\text{mm}, e = 0, \epsilon_{11} = 2500$ -strain

(b)  $w = 100\text{mm}, b = 20\text{mm}, \epsilon_{11} = 2500$ -strain

Fig. 10. Parametric evaluation of the SERR depending on the specimen width  $w$  and the damage eccentricity  $e$ . The test case equal to that in Fig. 8.

to one. The correctness of this approach can be questioned, as the real load distribution in the side sections is likely to be non-uniform with a peak next to the delamination edge. Nonetheless, the current work does not contain an investigation of non-uniform load distributions.

The second diagram in Fig. 10b depicts the behavior of the SERRs depending on the dimensionless eccentricity of the damage,  $\frac{e}{\frac{w}{2}-b}$ . This dimensionless parameter is zero for a centric damage and one for a damage placed at the specimen edge. The result is an increase of the SERR value  $G_y^l$ , on the side with the smaller undamaged width. The value on the opposite side,  $G_y^r$  is decreasing. This

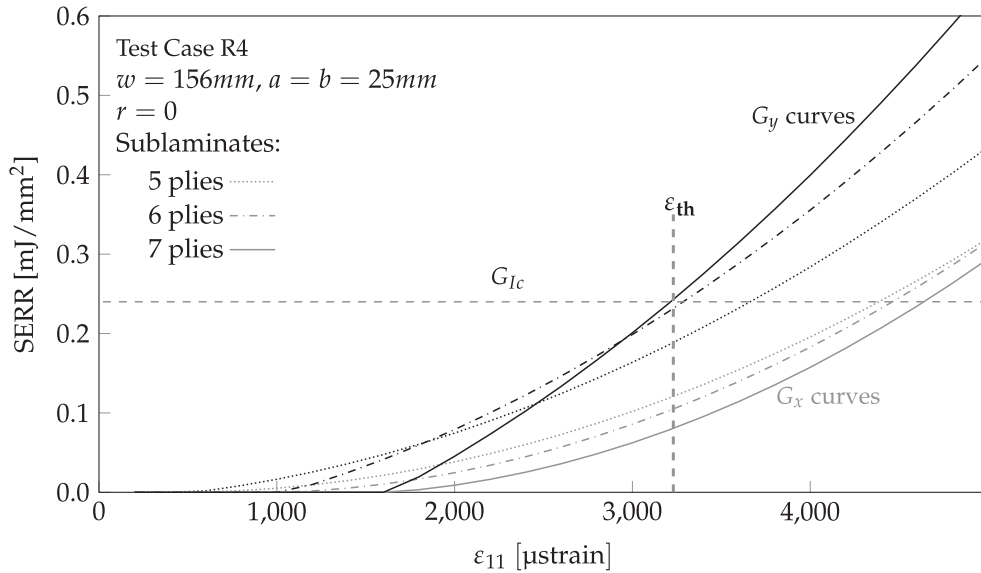


**Fig. 11.** SERR curves of test case R4 (HTA/6376 ZD from Rhead et al. [45]).  $\epsilon_{th}$  represents a conservative estimate of the laminate's residual capacity.

behavior is plausible, as the load transfer is more significant in the side section with the smaller width. The smaller cross section has to sustain a much larger load to balance the moments. Moreover, a slight increase of the value  $G_x$  can be observed for increasingly eccentric damage.

Eventually it turns out, that  $G_y^r$  becomes negative before the relative eccentricity approaches one which is not physically based but an artifact of the analysis method. First, a real damage is elliptical and the load redistribution is not discretely beginning at the damage tip but happening continuously throughout the delamination length. The assumption of a sudden load increase is likely to overshoot the real SERR increase. Second, the simplified calculation of the equilibrium of moments assumes constant sublaminates forces  $F_{sub}$ . Hence, the balance of moments is obtained through the shifting of force from the larger to the smaller side section. In fact, also the sublaminates force would increase due to the equilibrium of moments. Hence, the current calculation of the correction factors  $n_r$  and  $n_l$  results in too high values. Nonetheless, the resulting increased SERR on the smaller side section is a conservative estimate of the real value. Eventually, the validity of the model for high eccentricity is still questionable. In consequence, further validation of the eccentric damage model through experiments or a numerical high-fidelity simulation would be a useful future step. When appropriate validation data is available, the implementation of an improved equilibrium of moments would be a further subject of interest.

### 3.4. Determination of a strain allowable

The determination of a DT strain allowable in the preliminary aircraft design can be conducted through the method presented in this work. It requires the assumption of a DT-relevant delamination size, which has to be determined by empirical damage data or experimental or numerical analysis of the impact threat [61,62]. A delamination of the relevant size has to be placed at different interfaces in the laminate. Hence, for each sublaminates configuration an SERR response is obtained, as shown in the example in Fig. 11. The curves show the response of three sublaminates of the test case R4 (HTA/6376 ZD configuration from Rhead et al. [45]). Each sublaminates has a different buckling strain and its own SERR response curves. These curves feature their individual intersection with the critical SERR. That way, the laminate-specific minimum value  $\min(\{\epsilon_{th}^i\})$  with  $i = [1, n_{sublaminates}]$  can be determined, after the entire stacking has been analyzed. A thus obtained minimum could be the reference value for a damage tolerance strain allowable in the aircraft design. In the considered example of case R4, the 7-ply sublaminates with determines the threshold of 3270  $\mu$ strain.

Nonetheless, this allowable accounts only for the tolerance of delamination, it does not include potential fiber cracking, interfiber fracture or fatigue effects under cyclic loading. Furthermore the validity is limited to compression load. Under tensile load, the damage propagation is driven by different effects [63] and the allowable strain is likely to be considerably higher than under compression [26].

## 4. Conclusion

In this work, we presented the development of an analytical, energy-based method to determine the delamination propagation under compression load. The method is based on the sublaminates buckling as the driving damage propagation effect. The damage is simplified to its rectangular envelope and the virtual crack extension principle is applied to assess the damage propagation. Through the combination with an analytical plate-buckling formula, an efficient and flexible analysis approach is created. Using this method, the following outcomes were obtained:

- The analytical calculation of the SERRs in perpendicular and parallel direction to the load axis is possible.
- The load transfer from the delaminated laminate section to the pristine sections alongside is considered. This load transfer accounts for the specimen width and the damage eccentricity.
- The damage propagation strain derives from the exceeding of the critical SERR at any delamination edge. This strain can serve as a design allowable.
- The obtained results were compared with experimental data from the literature and affirm that the method conservatively predicts the threshold strain for crack propagation. Nonetheless, an existing semi-analytical method from the literature [45] results in quantitatively better predictions.

Hence, this approach permits the derivation of conservative strain allowables, as required within the sizing process of preliminary aircraft design. In this way, it permits the early phase consideration of delamination damage in composite laminates. Thus, the application of the method within a structural sizing process is a future subject of interest. Nonetheless, to achieve a valid damage-tolerant design in preliminary aircraft design, tensile loading and additional damage modes have to be considered.

Possible future improvements of the presented method could account for the elliptical delamination shape, a corresponding non-uniform load transfer, and varying distribution of the applied load. Furthermore, additional validation through experimental data or numerical high-fidelity analysis is useful with regard to two aspects, the directional dependency of the SERR and the influence of the damage eccentricity.

### Declaration of Competing Interest

The authors declare that they have no known competing financial interests or personal relationships that could have appeared to influence the work reported in this paper.

### Acknowledgements

All research was accomplished within the DLR project KonTeKst. The authors acknowledge the German Aerospace Center (DLR) for funding this project.

### Appendix A. Critical strain for sublaminare buckling

The analytical, two-dimensional DT method presented in this work is based on the sublaminare buckling, as the driving phenomenon to the crack tip opening. Hence, the method requires an analytical calculation of the critical strain for sublaminare buckling  $\varepsilon_c$ . A numerical calculation as proposed by Rhead et al. [45] through the tool VICONOPT [58] provides plausible results. Their combination of a numerical buckling analysis and an analytical evaluation of the delamination is superior to a purely analytical approach. Thus, the supplementation of analytical methods and numerical approaches often results in a combined method [64] which is more efficient than a comparable fully analytical or numerical method. However, a numerical calculation does not match the needs of preliminary aircraft design where the equations in an optimization loop have to be evaluated within a fraction of a second. Hence, either the numerical evaluation has to be conducted before the model is applied. With a predetermined response surface, the buckling strain could be determined through a surrogate model which is similarly fast as an analytical equation.

Alternatively, an analytical alternative has to replace the numerical part. For the present work, analytical plate buckling equations have been employed. The plate is represented by the rectangular envelope of the delamination with the dimensions  $2a \times 2b$ . Such equations for rectangular orthotropic plates with simply supported or built-in edges are available in the HSB in Section 45100 [4]. The Eqs. (A.1)–(A.5) describe the analytical method according to the HSB. This method finds on the bending stiffness  $\mathbf{D}$  calculated through the CLT and employs an empirical relation for the minimum envelope of the buckling curve. Depending on the boundary conditions, the parameters  $q$  and  $h$  in Eq. (A.4) are selected. Simply supported boundary conditions are represented by  $q = 2$  and  $h(\alpha) = \min_{m=1,2,\dots} \left[ \left( \frac{m}{\alpha} \right)^2 + \left( \frac{\alpha}{m} \right)^2 \right]$ . Built-in edges are described by  $q = 2.36$  and  $h$  through the diagram in the HSB Section 45111–08 [4].

$$\alpha = \frac{a}{b} \sqrt{\frac{D_{22}}{D_{11}}} \quad (\text{A.1})$$

$$\beta = \frac{D_{12} + 2D_{66}}{\sqrt{D_{11} \cdot D_{22}}} \quad (\text{A.2})$$

$$\eta = \frac{2 \cdot D_{66}}{\sqrt{D_{11} \cdot D_{22}}} \quad (\text{A.3})$$

$$k_x = h(\alpha) + q \cdot \beta \quad (\text{A.4})$$

$$n_{c,hsb} = k_x \left( \frac{\pi}{2b} \right)^2 \sqrt{D_{11} \cdot D_{22}} \quad (\text{A.5})$$

Moreover, some researchers propose analytical equations for the determination of the buckling strain in simply supported or clamped composite plates, for example, Tarján and Kollar [54]. The Eqs. (A.6) and (A.7) describe the plate buckling load for simply supported and built-in edges, respectively. The derivation of both equations is described in the referenced work (Eqs. (2) and (8), respectively).

$$n_{c,tarjan}^{simply} = \min \left[ \left( \frac{\pi}{2b} \right)^2 \left( D_{11} \left( \frac{2bi}{2a} \right)^2 + D_{22} \left( \frac{2a}{2bi} \right)^2 + 2(D_{12} + 2D_{66}) \right) \right] \quad (\text{A.6})$$

$$n_{c,tarjan}^{builtin} = \left( \frac{\pi}{2b} \right)^2 \left( 3.928D_{11} \left( \frac{2b}{2a} \right)^2 + 3.928D_{22} \left( \frac{2a}{2b} \right)^2 + 2.62(D_{12} + 2D_{66}) \right) \quad (\text{A.7})$$

The formulas from the HSB and Tarján are valid for symmetric orthotropic plates, where the coupling stiffness in the B matrix vanishes. In case of unsymmetrical laminates with a nonzero coupling matrix B, the corrected plate stiffness  $\tilde{\mathbf{D}}$  according to (A.8) has to be used instead of the bending stiffness  $\mathbf{D}$ . For symmetric orthotropic laminates is  $\tilde{\mathbf{D}} = \mathbf{D}$ .

$$\tilde{\mathbf{D}} = \mathbf{D} - \mathbf{B}^T \mathbf{A}^{-1} \mathbf{B} \quad (\text{A.8})$$

## References

- [1] H.K. Reddick, Safe-life and damage-tolerant design approaches for helicopter structures, *Fail. Anal. Mech. Failure of Fibrous Compos. Struct.* 2278 (1983) 129–151.
- [2] Federal Aviation Administration, F.A. Administration, AC 25.571-1D Damage tolerance and fatigue evaluation of structure, US Government Printing Officedoi:10.1177/00472875301200242.
- [3] S.M.O. Tavares, P.M.S.T.D. Castro, *Damage Tolerance of Metallic Aircraft Structures*, Cham, 2018. URL isbn: 978-3319701899.
- [4] IASB, *Handbuch Struktur Berechnung*, no. 2016, Struktur-Berechnungsunterlagen, Industrie-Ausschuss, 1976.
- [5] T.K. O'Brien, *Towards a damage tolerance philosophy for composite materials and structures*, Tech. Rep. March, NASA, Hampton, Virginia (1988).
- [6] J. Baaran, Study on visual inspection of composite structures EASA-Research Project/2007/3 - Final Report, Tech. rep., EASA (2009). URL [https://www.easa.europa.eu/sites/default/files/dfu/EASA\\_REP\\_RESEA\\_2007\\_3.pdf](https://www.easa.europa.eu/sites/default/files/dfu/EASA_REP_RESEA_2007_3.pdf).
- [7] G. Newaz, R.L. Sierakowski, *Damage Tolerance in Advanced Composites*, Taylor & Francis, 1995 [https://books.google.de/books?id=\\_hr1Ys1toA4C](https://books.google.de/books?id=_hr1Ys1toA4C).
- [8] Federal Aviation Administration, Advisory Circular: 20–107B - Composite Aircraft Structure.
- [9] EASA, AMC 20-29 Composite Aircraft Structure - Annex II to ED Decision 2010/003/R of 19/07/2010 (2010) 1–36.
- [10] P. Goudou, Decision No 2010/003/R of the executive director of the European Aviation Safety Agency, Tech. rep., Cologne (2010). URL [https://www.easa.europa.eu/sites/default/files/dfu/ED Decision 2010\\_003\\_R.pdf](https://www.easa.europa.eu/sites/default/files/dfu/ED Decision 2010_003_R.pdf).
- [11] G. Davies, P. Irving, 9 - Impact, post-impact strength and post-impact fatigue behaviour of polymer composites, in: *Polymer Composites in the Aerospace Industry*, Elsevier Ltd, 2015, pp. 231–259. doi:10.1016/B978-0-85709-523-7.00009-8.
- [12] L.G. Melin, J. Schön, Buckling behaviour and delamination growth in impacted composite specimens under fatigue load: An experimental study, *Compos. Sci. Technol.* 61 (13) (2001) 1841–1852, [https://doi.org/10.1016/S0266-3538\(01\)00085-9](https://doi.org/10.1016/S0266-3538(01)00085-9).
- [13] D.D. Symons, G. Davis, Fatigue testing of impact-damaged T300/914 carbon-fibre-reinforced plastic, *Compos. Sci. Technol.* 60 (2000) 379–389, [https://doi.org/10.1016/S0266-3538\(99\)00138-4](https://doi.org/10.1016/S0266-3538(99)00138-4).
- [14] N. Uda, K. Ono, K. Kunoo, Compression fatigue failure of CFRP laminates with impact damage, *Compos. Sci. Technol.* 69 (14) (2009) 2308–2314, <https://doi.org/10.1016/j.compotech.2008.11.031>.
- [15] M. Mitrovic, H.T. Hahn, G.P. Carman, P. Shyprykevich, Effect of loading parameters on the fatigue behaviour of impact damaged composite laminates, *Compos. Sci. Technol.* 59 (1999) 2059–2078, [https://doi.org/10.1016/S0266-3538\(99\)00061-5](https://doi.org/10.1016/S0266-3538(99)00061-5).
- [16] G. Davies, P. Irving, Impact, post-impact strength and post-impact fatigue behaviour of polymer composites, Elsevier Ltd, 2014, <https://doi.org/10.1016/B978-0-85709-523-7.00009-8>.
- [17] S. International, COMPOSITE MATERIALS HANDBOOK Volume 3 - Polymer Matrix Composites: Materials, Usage, Design, and Analysis, no. March, Wichita State University, 1994. URL <https://www.cmh17.org/>.
- [18] I. Papa, M.R. Ricciardi, V. Antonucci, A. Langella, J. Tirillò, F. Sarasini, V. Pagliarulo, P. Ferraro, V. Lopresto, Comparison between different non-destructive techniques methods to detect and characterize impact damage on composite laminates, *J. Compos. Mater.* 54 (5) (2019) 617–631, <https://doi.org/10.1177/0021998319864411>.
- [19] M. Moix-Bonet, B. Eckstein, P. Wierach, Probability - Based Damage Assessment on a Composite Door Surrounding Structure, in: 8th European Workshop On Structural Health Monitoring (EWSHM), no. July, Bilbao, Spain, 2016, pp. 5–8. <https://elib.dlr.de/117046/>.
- [20] S. Sikdar, S. Banerjee, *Structural Health Monitoring of Advanced Composites Using Guided Waves*, no. September, Lambert Academic Publishing, Beau Bassin, 2017. URL isbn: 978-620-2-02697-0.
- [21] G. Clark, T.J. Van Blaricum, Load spectrum modification effects on fatigue of impact-damaged carbon fibre composite coupons, *Composites* 18 (3) (1987) 243–251, [https://doi.org/10.1016/0010-4361\(87\)90414-9](https://doi.org/10.1016/0010-4361(87)90414-9).
- [22] A.T. Rhead, R. Butler, G.W. Hunt, Compressive strength of composite laminates with delamination- induced interaction of panel and sublaminates buckling modes, *Compos. Struct.* 171 (2017) 326–334, <https://doi.org/10.1016/j.compstruct.2017.03.011>.
- [23] T.A. Sebaey, E.V. González, C.S. Lopes, N. Blanco, J. Costa, Damage resistance and damage tolerance of dispersed CFRP laminates: Design and optimization, *Compos. Struct.* 95 (2013) 569–576, <https://doi.org/10.1016/j.compstruct.2012.07.005>.
- [24] N. Dubary, C. Bouvet, S. Rivallant, L. Ratsifandrihana, Damage tolerance of an impacted composite laminate, *Compos. Struct.* 206 (July) (2018) 261–271, <https://doi.org/10.1016/j.compstruct.2018.08.045>.
- [25] A. Nettles, A. Hodge, J. Jackson, An examination of the compressive cyclic loading aspects of damage tolerance for polymer matrix launch vehicle hardware, *J. Compos. Mater.* 45 (4) (2011) 437–458, <https://doi.org/10.1177/0021998310376117>.
- [26] R. Bogenfeld, P. Schmiedel, N. Kuruvadi, T. Wille, J. Kreikemeier, An experimental study of the damage growth in composite laminates under tension–fatigue after impact, *Compos. Sci. Technol.* 191 (May). doi:10.1016/j.compotech.2020.108082.
- [27] M. Abir, T. Tay, M. Ridha, H. Lee, On the relationship between failure mechanism and compression after impact (CAI) strength in composites, *Compos. Struct.* 182 (July) (2017) 242–250, <https://doi.org/10.1016/j.compstruct.2017.09.038>.
- [28] C.P. Dielen, T. Qaimari, A Finite Element Study on the Influence of Delamination Shape on Residual Compressive Behavior of Single and Multiple Delaminated Composite Structures, *Proceedings of the 5th International Workshop on Aircraft System technologies*, Shaker Verlag Aachen, Hamburg, 2015, pp. 335–344.
- [29] A. Riccio, GARTEUR AG-32: Damage Growth in Composites Final Report TP-176, Tech. rep., Second University of Naples (2012).
- [30] C.P. Dielen, H. Meyer, M. Werwer, C. Willberg, Estimation of airframe weight reduction by integration of piezoelectric and guided wave-based structural health monitoring, *Struct. Heal. Monit.* doi:10.1177/1475921718813279.
- [31] Airbus Industries, AITM 1–0010 Determination of Compression Strength After Impact (2005).

- [32] Y. Feng, Y. He, H. Zhang, X. Tan, T. An, J. Zheng, Effect of fatigue loading on impact damage and buckling/post-buckling behaviors of stiffened composite panels under axial compression, *Compos. Struct.* 164 (2017) 248–262, <https://doi.org/10.1016/j.compstruct.2016.12.069>.
- [33] T. Führer, C. Willberg, S. Freund, F. Heinecke, Automated model generation and sizing of aircraft structures, *Aircraft Eng. Aerosp. Technol.* 88 (2) (2016) 268–276, <https://doi.org/10.1108/AEAT-02-2015-0054>.
- [34] T. Klimmek, M. Schulze, M. Abu-Zurayk, C. Ilic, A. Merle, Cpacs-Mona-an Independent and in High-Fidelity Based Mdo Tasks Integrated Process for the Structural and Aeroelastic Design of Aircraft Configurations (June) (2019) 1–21. URL <https://elib.dlr.de/127930/1/IFASD-2019-028.pdf>.
- [35] P. Paris, F. Erdogan, A Critical Analysis of Crack Propagation Laws, *J. Fluids Eng.* 85 (4) (1963) 528–533, <https://doi.org/10.1115/1.3656900>.
- [36] R. Krueger, Development of a Benchmark Example for Delamination Fatigue Growth Prediction, *Fatigue Compos. Mater.* 3 (2010) 54–73 <http://www.amazon.co.uk/Development-Benchmark-Example-Delamination-Prediction/dp/1234056755>.
- [37] A.J.-M. Gbaguidi, Fatigue Damage Prognosis of Internal Delamination in Composite Plates Under Cyclic Compression Loadings Using Affine Arithmetic as Uncertainty Propagation Tool, Ph.D. thesis Embry-Riddle Aeronautical University, 2014.
- [38] J.B. Chang, V.K. Goyal, J.C. Klug, J.I. Rome, Composite Structures Damage Tolerance Analysis Methodologies, Tech. Rep. March 2012, NASA, El Segundo (2012).
- [39] F.-R. P.M. Composites, Standard Test Method for Mode I Interlaminar Fracture Toughness of Unidirectional 01 (Reapproved 2007) (2013) 1–12. doi:10.1520/D5528-01R07E03.2.
- [40] Airbus Industrie, AITM 1-0006 Carbon fiber reinforced plastic - Interlaminar fracture toughness energy Mode II (1994).
- [41] R.S. Choudhry, A.T. Rhead, M.W. Nielsen, R. Butler, A plate model for compressive strength prediction of delaminated composites, *Compos. Struct.* 210 (October 2018) (2019) 509–517, <https://doi.org/10.1016/j.compstruct.2018.11.066>.
- [42] C.P. Dielen, T. Wille, J.G. Santafe, A new method for individual impact damage and repair assessment on composite structures based on residual strength analysis, *Greener Aviation Conference* (1) (2016) 1–8.
- [43] A. Riccio, A. Sellitto, R. Ricchiuto, Delamination Growth in Composite Plates Under Fatigue Loading Conditions, in: *Damage Growth in Aerospace Composites*, Springer International Publishing, 2015, p. 124. doi:10.1007/978-3-319-04004-2\_4 89. [http://link.springer.com/10.1007/978-3-319-04004-2\\_4 89. http://link.springer.com/10.1007/978-3-319-04004-2\\_6](http://link.springer.com/10.1007/978-3-319-04004-2%0Ahttp://link.springer.com/10.1007/978-3-319-04004-2_6).
- [44] A. Köllner, F. Forsbach, C. Völlmecke, Delamination Buckling in Composite Plates: an Analytical Approach to Predict Delamination Growth, Springer International Publishing, Cham, 2019, pp. 241–255, [https://doi.org/10.1007/978-3-030-13307-8\\_18](https://doi.org/10.1007/978-3-030-13307-8_18).
- [45] A.T. Rhead, R. Butler, G.W. Hunt, Post-buckled propagation model for compressive fatigue of impact damaged laminates, *Int. J. Solids Struct.* 45 (2008) 4349–4361, <https://doi.org/10.1016/j.ijsolstr.2008.03.014>.
- [46] A.T. Rhead, R. Butler, Compressive static strength model for impact damaged laminates, *Compos. Sci. Technol.* 69 (14) (2009) 2301–2307, <https://doi.org/10.1016/j.compscitech.2009.01.010>.
- [47] A.T. Rhead, Analysis and optimisation of post buckled damage tolerant composite laminates, Ph.D. thesis University of Bath, 2009.
- [48] R. Butler, A.T. Rhead, W. Liu, N. Kontis, C. Down, Compressive strength of delaminated aerospace, *Philos. Trans. R. Soc. London* 370 (2012) 1759–1779, <https://doi.org/10.1098/rsta.2011.0339>.
- [49] M.L. Benzeggagh, M. Kenane, Measurement of mixed-mode delamination fracture toughness of unidirectional glass/epoxy composites with mixed-mode bending apparatus, *Compos. Sci. Technol.* 56 (4) (1996) 439–449, [https://doi.org/10.1016/0266-3538\(96\)00005-X](https://doi.org/10.1016/0266-3538(96)00005-X).
- [50] A. Griffith, The Phenomena of Rupture and Flow in Solids, *Philos. Trans. R. Soc. Lond.* 221 (1921) 163–198.
- [51] M.J. Pavier, W.T. Chester, Compression failure of carbon fibre-reinforced coupons containing central delaminations, *Composites* 21 (1) (1990) 23–31, [https://doi.org/10.1016/0010-4361\(90\)90095-E](https://doi.org/10.1016/0010-4361(90)90095-E).
- [52] C.G. Diaconu, P.M. Weaver, Approximate Solution and Optimum Design of Compression-Loaded, Postbuckled Laminated Composite Plates, *Int. J. Solids Struct.* 43 (4) (2005) 6978–6997, <https://doi.org/10.2514/1.10827>.
- [53] E. Werthen, S. Dähne, Design- and Manufacturing Constraints within the Gradient Based Optimization of a Composite Aircraft Wingbox, in: 6th Airframe Structural Design Conference, no. October, Bristol, 2018.
- [54] G. Tarján, L.P. Kollár, Buckling of axially loaded composite plates with restrained edges, *J. Reinf. Plast. Compos.* 29 (23) (2010) 3521–3529, <https://doi.org/10.1177/0731684410381153>.
- [55] A.T. Rhead, R. Butler, W. Liu, N. Baker, The influence of surface ply fibre angle on the compressive strength of composite laminates containing delamination, *Aeronaut. J.* 116 (1186) (2012) 1315–1330, <https://doi.org/10.1017/S000192400000765X>.
- [56] A.S. Chen, D.P. Almond, B. Harris, In situ monitoring in real time of fatigue-induced damage growth in composite materials by acoustography, *Compos. Sci. Technol.* 61 (16) (2001) 2437–2443, [https://doi.org/10.1016/S0266-3538\(01\)00165-8](https://doi.org/10.1016/S0266-3538(01)00165-8).
- [57] L.G. Melin, J. Schön, Buckling behaviour and delamination growth in impacted composite specimens under fatigue load: An experimental study, *Compos. Sci. Technol.* 61 (13) (2001) 1841–1852, [https://doi.org/10.1016/S0266-3538\(01\)00085-9](https://doi.org/10.1016/S0266-3538(01)00085-9).
- [58] F.W. Williams, D. Kennedy, M.S. Anderson, R. Butler, VICONOPT - Program for exact vibration and buckling analysis or design of prismatic plate assemblies, *AIAA J.* 29 (11) (1991) 1927–1928, <https://doi.org/10.2514/3.10820>.
- [59] M. Ilyas, F. Lachaud, C. Espinosa, M. Salauin, Dynamic delamination of aeronautic structural composites by using cohesive finite elements, in: 17th International Conference on Composite Materials (ICCM-17), Edinburgh, GB, 2009, pp. 27–31. URL <https://oatao.univ-toulouse.fr/3537/>.
- [60] B.G. Falzon, S.C. Hawkins, C.P. Huynh, R. Radjef, C. Brown, An investigation of Mode I and Mode II fracture toughness enhancement using aligned carbon nanotubes forests at the crack interface, *Compos. Struct.* 106 (2013) 65–73, <https://doi.org/10.1016/j.compstruct.2013.05.051>.
- [61] R. Bogenfeld, J. Kreikemeier, T. Wille, An analytical scaling approach for low-velocity impact on composite structures, *Compos. Struct.* 187 (2018) 71–84, <https://doi.org/10.1016/j.compstruct.2017.12.012>.
- [62] R. Matadi Boumbimba, C. Froustey, P. Viot, P. Gerard, Low velocity impact response and damage of laminate composite glass fibre/epoxy based tri-block copolymer, *Compos. Part B: Eng.* 76 (2015) 332–342, <https://doi.org/10.1016/j.compositesb.2015.02.007>.
- [63] V.V. Bolotin, Delaminations in composite structures: its origin, buckling, growth and stability, *Compos. Part B* 95 (1996) 129–145, [https://doi.org/10.1016/1359-8368\(95\)00035-6](https://doi.org/10.1016/1359-8368(95)00035-6).
- [64] B. Weigand, R. Bogenfeld, A solution to the turbulent Graetz problem by matched asymptotic expansions for an axially rotating pipe subjected to external convection, *Int. J. Heat Mass Transf.* 78 (November) (2014) 901–907, <https://doi.org/10.1016/j.ijheatmasstransfer.2014.07.057>.